J|A|C|S
ARTICLES
Published on Web 06/18/2003

Encapsulated Oxide Nanoparticles: The Influence of the Microstructure on Associated Impurities within a Material

Dean C. Sayle*,† and Stephen C. Parker‡

Contribution from the Department of Environmental and Ordnance Systems, Cranfield University, Royal Military College of Science, Shrivenham, Swindon, U.K., SN6 8LA, and Department of Chemistry, University of Bath, Claverton Down, Bath, Avon, U.K., BA2 7AY

Received February 20, 2003; E-mail: sayle@rmcs.cranfield.ac.uk

Abstract: Simulation techniques have been used to explore how the microstructure of a material influences the nature of associated impurities embedded therein. We illustrate this by exploring four systems: BaO and CaO nanoparticles encapsulated within a ("perfect") MgO host lattice and SrO and MgO nanoparticles encapsulated within a ("microstructural") BaO lattice, which comprises a network of screw-edge dislocations. This study uses annealing techniques to generate energetically feasible nanoparticle structures and morphologies, dislocation networks, interfacial boundaries, and strain profiles. Specifically, the different encapsulated nanoparticles exhibit a range of morphologies, expose a variety of facets at the nanoparticle/host lattice interface, and are observed to rotate within the cavity they occupy inside the host lattice. The structure and nature of the nanoparticles reflect the lattice misfit between the nanoparticle and the host lattice. The study suggests also that there exists a "critical nanoparticle size", above which dislocations evolve.

Introduction

As the size of a material reduces to the nanometer scale, the structure and properties change uniquely in comparison with those of the bulk.[1,2] Such phenomena offer the promise of "new" materials and properties and have spawned the field of nanoscience.[3]

One particular area within nanoscience is the embedding of nanoparticles within a host material. For example, various materials have been encapsulated within porous host lattices such as zeolites,[4] where the zeolitic channel sizes fall within the nanoparticle region. More recently, materials have been successfully encapsulated within single and multiwall carbon nanotubes, leading to the fabrication of one-dimensional materials.[5] The intense scientific interest in these systems is hardly surprising since, by suitable choice of encapsulating lattice, one can exact control over both the structure and properties of the encapsulated material (for example see ref 6); methods for controllable nanoparticle synthesis are available.[7] One can also envisage encapsulation of a nanoparticle within a "fully dense" host lattice. Indeed, Jeng and Shen have explored the structure of NiO nanoparticles encapsulated within CaO by sintering and annealing NiO and CaO powders, and van Huis et al. and van Veen et al. have explored silver and gold nanoclusters embedded in the near surface regions of MgO[8] and nanocavity formation processes in MgO[9] using ion implantation techniques.

When impurities are introduced into a material, at one limit they can bind to point defect impurities[10] and at the other extreme form nanocrystals, i.e., not true solid solutions, but micromixtures, clearly, an important issue since the nature of such impurities will reflect upon the material properties. Moreover, whether such impurities are dispersed or aggregated to form nanoparticles is likely governed by the microstructure of the material in which they inhabit. For example, defects have been observed to segregate to grain-boundary regions within a material.[11−13] In addition, if nanoparticles are formed, the extent to which they will be amorphous or crystalline needs to be determined.

In previous work we have developed simulation strategies to explore the microstructure of supported nanoparticles and thin films. In particular, we have successfully generated atomistic models, which comprise all the major (experimentally observed) microstructural features within a single *mesoscopic* model. This rich microstructure includes, for example, disloca-

† Cranfield University.
‡ University of Bath.

(1) Gleiter, H. *Acta Mater.* **2000**, *48*, 1.
(2) Pardoe, H.; Chua-anusorn, W.; St. Pierre, T. G.; Dobson, J. *J. Magn. Magn. Mater.* **2001**, *225*, 41.
(3) Rao, C. N. R.; Cheetham, A. K. *J. Mater. Chem.* **2001**, *11*, 2887.
(4) Viswanadham, N.; Shido, T.; Iwasawa, Y. *Appl. Catal. A* **2001**, *219*, 223.
(5) Monthioux, M. *Carbon* **2002**, *40*, 1809.
(6) Kim, Y.; Yoon, M. *J. Mol. Catal. A* **2001**, *168*, 257.
(7) O'Brien, S.; Brus, L.; Murray, C. B. *J. Am. Chem. Soc.* **2001**, *123*, 12085.
(8) Van Huis, M. A.; Fedorov, A. V.; van Veen, A.; Falub, C. V.; Eijt, S. W. H.; Kooi, B. J.; De Hosson, J. Th. M.; Hibma, T.; Zimmerman, R. L. *Nucl. Instrum. Methods Phys. Res. B* **2002**, *191*, 442.
(9) van Veen, A.; van Huis, M. A.; Fedorov, A. V.; Schut, H.; Labohm, F.; Kooi, B. J.; De Hosson, J. Th. M. *Nucl. Instrum. Methods Phys. Res. B* **2002**, *191*, 610.
(10) Duffy D. M. *J. Phys.* **1986**, *C19*, 4393.
(11) Yoshida, H.; Ikuhara, Y.; Sakuma, T. *Acta Mater.* **2002**, *50*, 2955.
(12) Harris, D. J.; Khan, M. A.; Parker, S. C. *Phys. Chem. Min.* **1999**, *27*, 133.
(13) Harris, D. J.; Watson, G. W.; Parker, S. C. *Phys. Rev. B* **1997**, *56*, 11477.

10.1021/ja030119i CCC: $25.00

tion networks,[14] grain boundaries,[15] lattice slip,[14] epitaxial configurations,[16] surface morphologies[17] comprising a wealth of surfaces exposed (including those associated with a dipole normal to the surface),[18] low interfacial densities, and ion migration across the interface. An obvious extension to this work is to use these models, as a framework, to establish the effect of this microstructure on the nature of impurities within the material and forms the basis of this present study.

The best way of investigating the location and environment of impurity or dopant species within nanoparticles is to use a combination of simulation and experiment such as EXAFS (as demonstrated by Rush et al.[19]). Clearly, partnership of experiment and theory affords a very powerful tool in understanding impurity segregation and structure. For example, these simulations will provide data that can be checked experimentally, e.g., bond distances and radial distribution functions, thereby acting additionally as a validation for the simulations performed.

We envisage two related areas of study to understand the influence of the microstructure on the nature of impurities. First, dispersed impurities within a particular microstructure[12,13,20] and, second, aggregated impurities within a particular microstructure. In this present study, we consider the latter.

In the first part of this study we describe our simulation strategy, which can be employed to explore the structure of aggregated impurities, or nanoparticles, within a host lattice. And in the second part, we use these techniques to simulate encapsulated nanoparticles within a "perfect" (bulk) host lattice and within a host lattice comprising a complex microstructure. Because the simulation enables us to generate low-energy structures, the various structural features and configurations will be energetically viable. Accordingly, the results will help us understand several important issues, including the following:

- **Aggregation or Dispersion of Impurity Species.** Will the nanoparticles dissolve to form a solid solution within the host lattice? If they do not dissolve, to what extent will they remain amorphous or will they recrystallize?
- **Structural and Morphological Features:** dislocation or grain-boundary evolution within the nanoparticle and host lattice; the nature of voids at the nanoparticle/host lattice interfaces; orientational relationships between the nanoparticle and encapsulating host; point defect evolution (vacancies, interstitials, substitutionals); morphological appearance and surfaces expressed by the nanoparticle.
- **Stress Profiles.** The introduction of a nanoparticle into a host lattice will introduce stresses within the material, which may influence strongly the mechanical and fatigue properties of a material;[21] an understanding of the microstructure of oxide/oxide composites and how they influence the strength of the material is of considerable technological importance.

Theoretical Methods

Potential Models. All the calculations presented in this study are based upon the Born model for ionic solids. In particular the interactions between all the ions within the system comprise long-range Coulombic terms with full ionic charges assigned to the ions. The Coulombic interactions are countered by short-range repulsive interactions, of the Buckingham form. Parameters for the interactions are taken from Lewis and Catlow.[22] In addition a rigid ion model is employed to reduce considerably the computational cost.

Generation of Encapsulated Nanoparticles. The strategy for generating an encapsulated nanoparticle within (a) a perfect material and (b) a material that includes a complex microstructure was achieved using the following procedure (Figure 1):

(1) *Generate substrate*: region I (colored blue), region II (white);
(2) *Generate host lattice*: place thin film (yellow) on top of substrate;
(3) *Amorphize thin film:* thin film (red/yellow);
(4) *Introduce nanoparticle*;
(5) *Anneal (recrystallize).*

(a) Perfect Host Lattice. To generate a perfect host lattice, the thin film comprises the same (oxide) material as the substrate. Accordingly, upon recrystallization, the system will facilitate a simple extension of the perfect material within the thin film (Figure 1).

(b) Microstructural Host. Conversely, to generate a microstructural host lattice, the thin film comprises a different material from that of the substrate. Here, the effect of the lattice misfit between the thin film and underlying substrate results in the formation of a wealth of structural features (microstructure).[23] Moreover, the simulation procedure can be manipulated to generate a variety of microstructures (i.e., dislocation networks or polycrystalline thin films comprising a wealth of grain boundaries and grain junctions[15]). In this present study, the simulation is directed toward generating a microstructure comprising a complex network of dislocations (Figure 1).

We consider four systems: CaO and BaO encapsulated within a perfect MgO host lattice and MgO and SrO encapsulated in a host lattice (BaO), which comprises a complex microstructure. A further feature of our simulation cells arises from the fact we recognize that the solubility of the impurities may be different at the surface compared to the bulk. Thus in keeping with our strategy of including sufficient complexity for the system to explore configurational space, we insert the nanoparticle near a surface. Thus, for example, if the impurities prefer (energetically) to wet the surface, then they can do so. We now describe in more detail the procedure (1−5 above) as applied to each of the four systems.

(1) Generate Substrate. A block of MgO, $8 \times 56 \times 56 = 25\,088$ atoms (along [001], [010], and [100], respectively) in size, was constructed with the top two MgO(002) layers assigned to region I and the bottom six MgO(002) layers held in region II; [001] is along the surface normal. This strategy uses what is now a very standard two-region simulation approach:[24] Ions in region I are allowed to relax explicitly, while those in region II are held fixed to ensure the correct crystalline environment for region I species. The simulations in this study were all performed within the framework of the DL_POLY code,[25] which employs three-dimensional periodic boundaries, and therefore images of the system are generated along [100], [010], and [001]. To create the surface, a void, sufficiently large to eliminate any artificial interactions between neighboring images, was introduced along [001].

(2) Generate Host Lattice. A thin film of MgO, $8 \times 56 \times 56 = 25\,088$ atoms in size, was then placed on top of the substrate to represent

(14) Sayle, D. C.; Watson, G. W. *Phys. Chem. Chem. Phys.* **2000**, *2*, 5491.
(15) Sayle, D. C.; Watson, G. W. *J. Mater. Chem.* **2000**, *10*, 2241.
(16) Sayle, T. X. T.; Catlow, C. R. A.; Sayle, D. C.; Parker S. C.; Harding, J. H. *Philos. Mag. A* **1993**, *68*, 565.
(17) Sayle, D. C.; Doig, J. A.; Maicaneanu, S. A.; Watson, G. W. *Phys. Rev. B* **2002**, *65*, 245414.
(18) Sayle, D. C.; Maicaneanu, S. A.; Watson, G. W. *J. Am. Chem. Soc.* **2002**, *124*, 11429.
(19) Rush, G. E.; Chadwick, A. V.; Kosacki, I.; Anderson, H. U. *Radiat. Eff. Defects Solids* **2001**, *156*, 117.
(20) Sayle, D. C.; Watson, G. W. *J. Phys. Chem. B* **2002**, *106*, 3778.
(21) Dye, D.; Stone, H. J.; Reed, R. C. *Curr. Opin. Solid State Mater. Sci.* **2001**, *5*, 31.
(22) Lewis, G. V.; Catlow, C. R. A. *J. Phys. C: Solid State Phys.* **1985**, *18*, 1149.
(23) Sayle, D. C.; Watson, G. W. *Surf. Sci.* **2001**, *473*, 97. Sayle, D. C.; Doig, J. A.; Parker, S. C.; Watson, G. W. Submitted for publication.
(24) Watson, G. W.; Kelsey, E. T.; DeLeeuw, N. H.; Harris D. J.; Parker, S. C. *J. Chem. Soc., Faraday Trans.* **1996**, *92*, 433.
(25) Smith W.; Forester, T. R. *The DL_POLY Molecular Simulation Package*; URL: http://www.dl.ac.uk/TCSC/Software/DL_POLY.

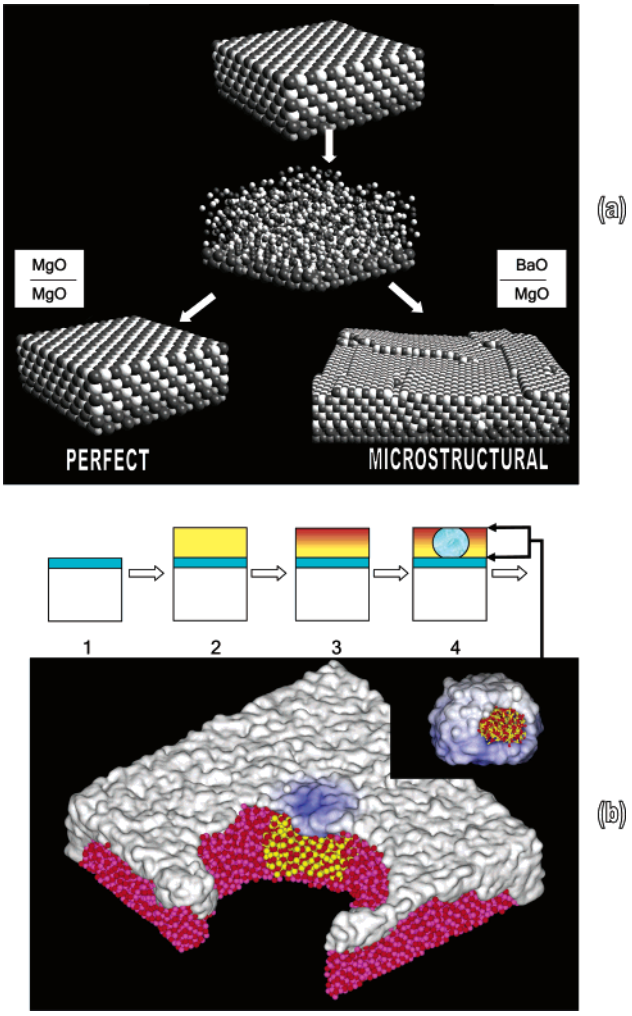

Figure 1. (a) Schematic illustrating the amorphization and recrystallization strategy. The initial configuration (top) is amorphized (middle). We find that after annealing the MgO/MgO system recrystallizes to give a perfect MgO host (bottom left), whereas the BaO/MgO system recrystallizes to give a microstructural BaO host (bottom right). The next step is to introduce a nanoparticle into either the MgO host (MgO/MgO) or the BaO host (BaO/MgO) as shown in (b) (the nanoparticle is introduced into the amorphous host); (b) top, schematic illustrating the simulation strategy used to generate models of encapsulated nanoparticles: (1) generate substrate; (2) place thin film (yellow) on substrate; (3) amorphize thin film; (4) introduce nanoparticle and finally anneal the system. The figure below shows the amorphous atomistic structures of the encapsulated nanoparticle within the host lattice; the lattice has been cut away to show more clearly the nature of the encapsulation. The inset shows the (amorphous) encapsulated nanoparticle only. Anions are colored red, cations (nanoparticle) are yellow, and cations (host lattice) are purple. Surface rendering is added to the schematics to aid visualization.

the host lattice. These ions are also held within region I and are allowed to relax explicitly under dynamical simulation. Thus far we have just constructed the starting configuration. In the following sections dynamical simulation is employed to direct the ions into low-energy configurations.

(3) Amorphize Thin Film. The MgO thin film (host lattice) was then amorphized. This was achieved by replacing all the Mg ions within the thin film by Ba. This, in effect, results in a BaO thin film supported on an MgO substrate. Since the lattice parameter for the BaO is 5.51 Å and that of MgO is 4.20 Å, the system is associated with a bulk 28% lattice misfit, F_B, following

$$F_B = \frac{2(a_{BaO} - a_{MgO})}{a_{BaO} + a_{MgO}} \quad (1)$$

Table 1. Procedure Employed for Generating the Various MO (nanoparticle) in M′O (thin film host)/MgO (substrate) Systems (M = Mg, Ca, Sr, Ba)[a]

system	nanoparticle (inside)	host lattice (outside)	MD (1000 K)	MD (0 K)
BaO in MgO/MgO	Ba	Mg	450	150
CaO in MgO/MgO	Ca	Mg	545	60
SrO in BaO/MgO	Sr	Ba	650	175
MgO in BaO/MgO	Mg	Ba	440	300

[a] For each system, the timings (ps) for the dynamical simulation (MD) at 1000 and 0 K are presented.

where a_{BaO} is the lattice parameter of BaO (5.51 Å) and a_{MgO}, the lattice parameter for MgO (4.20 Å). Accordingly, for this configuration, the BaO thin film is compressed, C, by 24% following

$$C = \frac{a_{BaO} - a_{MgO}}{a_{BaO}} \quad (2)$$

This 24% compression is sufficient to induce an amorphous transition on the (BaO) thin film under dynamical simulation.[14] Dynamical simulation was performed on the system for 2 ps at 1200 K, which resulted in an amorphous transition as the BaO lattice attempts to quench the considerable stress within the system. Preliminary tests on the system revealed that 2 ps was sufficient to amorphize the thin film without initiating any recrystallization. The calculated radial distribution functions showed no long-range order, indicating the amorphous nature of the system after 2 ps. It was anticipated that any recrystallization prior to introducing the nanoparticle would be detrimental, as regions that had recrystallized would hinder ionic mobility.

Amorphizing the system enables the potential energy barriers associated with ion migration to be lowered considerably compared with the crystalline material. Consequently, the ions have sufficient mobility to rearrange into low-energy configurations within the short time scales (generally on the order of nanoseconds) accessible to typical dynamical simulations. Indeed, the mobility is similar to that observed within a melt,[23] enabling appreciable exploration of the potential energy surface, using current computational resources. Conversely, dynamical simulation, as applied to a crystalline ionic solid, would give no appreciable ionic mobility; rather, the ions would simply vibrate about their lattice positions.

(4) Introduce Nanoparticle. The next step was to introduce the nanoparticle into the amorphous BaO lattice. Accordingly, a sphere of radius 20 Å and centered at the middle of the amorphous BaO thin film was constructed. The final configuration is therefore an amorphous thin film supported on an MgO substrate with a central amorphous "nanoparticle" region (Figure 1).

Within the sphere the (688) cations can then be exchanged with cations comprising the nanoparticle, and outside the sphere the (11 856) cations can be exchanged with cations comprising the host matrix. The strategy was to generate a *general* starting configuration, from which a variety of permutations of systems could be constructed as opposed to the time-consuming procedure of constructing a new amorphized cell for each system. We consider four systems in this present study, which were constructed by a simple exchange of cations following Table 1.

(5) Anneal. Each system was then annealed by performing dynamical simulation for long duration (timings given in Table 1). The duration of the dynamical simulations was sufficiently long to ensure that the systems were no longer evolving structurally nor energetically. Finally, dynamical simulation, performed at 0 K, was performed to effectively energy minimize each system.

Results

In each study we found that to understand the atomistic structure of the encapsulated nanoparticles and host lattice, graphical techniques needed to be used extensively throughout.

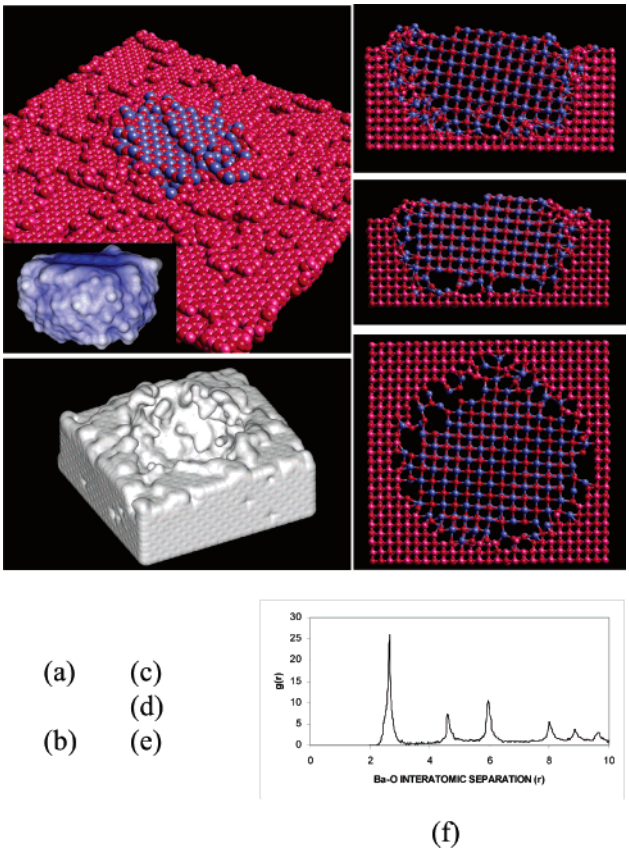

Figure 2. (a) Sphere model representation of the surface of the simulation cell for the BaO nanoparticle encapsulated within a perfect MgO host lattice. Inset shows the morphological appearance of the BaO nanoparticle only; (b) surface rendering model of part of the simulation cell showing the void that the BaO nanoparticle occupies; (c−e) thin slices cut through the system and viewed along [100], [010], and [001], respectively; (f) calculated Ba−O radial distribution function (RDF). Oxygen is colored red, barium is blue, and magnesium is purple.

For each of the four systems considered, various images are depicted, showing the atom positions for the final recrystallized structures. One of the clear results was that in each case the amorphous particles recrystallized to form small, fairly defect-free particles with comparatively small interphase regions. We now explore each system in turn and reflect upon the orientational, epitaxial, stress profile, dislocation, grain-boundary, and defect structures associated with each system. In this first section we consider the nature of nanoparticles encapsulated within a "perfect" host lattice. Specifically, we consider BaO encapsulated within MgO followed by CaO encapsulated in MgO.

BaO in MgO(perfect)/MgO(001); +28% Misfit. The results depicted in Figure 2 show the BaO nanoparticle encapsulated within a perfect MgO host lattice. A sphere model representation of the atom positions, depicting the surface of the MgO together with the BaO nanoparticle (center), is shown in Figure 2a. The surface structure is highly complex and comprises monatomic surface steps and ledges at the surface of both the host MgO lattice and BaO nanoparticle. Figure 2a (inset) depicts the morphological appearance of the BaO nanoparticle alone, the encapsulating MgO lattice having been removed to improve clarity. Figure 2b shows part of the encapsulating MgO lattice with the BaO nanoparticle removed to show the void that it occupies. It is clear from this image that the MgO lattice envelopes the BaO nanoparticle at the surface.

The orientation of the resulting BaO nanoparticle with respect to the encapsulating lattice was examined by cutting thin slices through the system along [100], [010], and [001], and these are shown in Figure 2, parts c−e, respectively. The figure demonstrates that both the MgO and BaO have recrystallized back into the rocksalt structure. However, the BaO is slightly misoriented with respect to the host MgO lattice. In particular, the nanoparticle is observed to have rotated by 8°, 6°, and 3° about [100], [010], and [001], respectively. Accordingly, one can assign interfaces between the two oxides as vicinal BaO{100}/MgO{100}.

It is clear from Figure 2c−e that the lattice planes of the BaO nanoparticle are not in alignment with the encapsulating MgO lattice. This is perhaps not surprising, since the bulk lattice misfit for this system is +28% (eq 1); clearly, for such a high lattice misfit, the energy associated with bringing the lattices into alignment would be considerable. The analysis of these simulations also reveals the mechanism for removing this large misfit: Inspection of Figure 2c shows that approximately 3 BaO(200) interplanar distances match with 4 MgO(200). This configuration is associated with a lattice misfit of about −1% (neglecting the small rotation of the BaO with respect to the MgO) following

$$F_{\mathrm{NCSL}} = \frac{2(na_{\mathrm{BaO}} - ma_{\mathrm{MgO}})}{na_{\mathrm{BaO}} + ma_{\mathrm{MgO}}} \qquad (3)$$

where F_{NCSL} is the misfit associated with the particular near coincidence site lattice (NCSL, see refs 16,26), a_{BaO} and a_{MgO} are the lattice parameters of the BaO and MgO lattices, respectively, and n (=3) and m (=4) are the number of (200) interplanar distances between coincident sites. This is not an unreasonable configuration since the strain energy associated with this −1% misfit is much lower than the "bulk" (28%) misfit. The epitaxial configuration assigned implies the presence of an "array" of misfit dislocations with periodicity approximately 8.8 Å ($4a_{\mathrm{MgO}}/2$).

Inspection of the internal regions of the BaO nanoparticle (Figure 2c−e) reveals no defects. Conversely, the interfacial regions (1−2 layers) are highly defective: substitutionals, "vacancies", and "interstitials" together with complex point defect clusters are observed to have evolved. In addition, the density of ions at the interfacial regions appears to be reduced. While the presence of substitutionals is clear, it is perhaps disingenuous to assign the terms "interstitials" and "vacancies" to the defects since the relaxation and perturbation of the crystals at the interfacial regions is considerable.

The strain profile within the nanoparticle was explored further by calculating the Ba−O radial distribution function and is presented in Figure 2f. The trace reveals that the "average" nearest neighbor Ba−O distance is 2.65 Å. Since the natural Ba−O bond distance is about 2.77 Å, the nanoparticle is (on average) slightly compressed compared to the parent material. However, the nearest neighbor peak is broad; Ba−O distances range from 2.3 to 3.2 Å. Clearly, some Ba−O distances (at the lower limit) are considerably shorter compared with the parent oxide, and therefore these regions suffer considerable compression. Conversely, others (at the upper limit) are elongated, indicating regions under tension. The calculated nearest neighbor

(26) Sutton, A. P.; Balluffi, R. W. *Acta Metall.* **1987**, *35*, 2177.

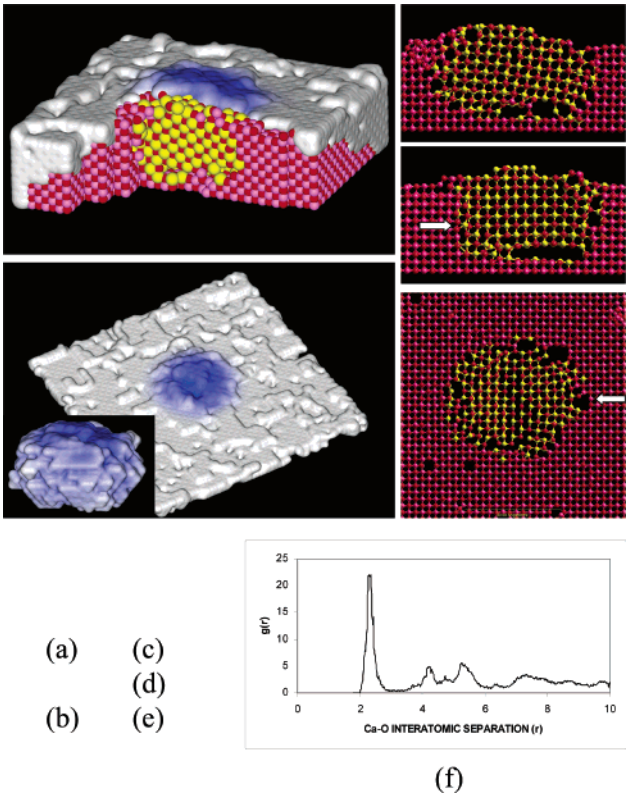

Figure 3. (a) Sphere model representation of the surface region of the simulation cell for the CaO nanoparticle encapsulated within a perfect MgO host lattice; (b) surface rendering model of the uppermost layers of the simulation cell (nanoparticle morphology inset); (c−e) thin slices cut through the system and viewed along [100], [010], and [001], respectively; (f) calculated Ca−O RDF. Oxygen is colored red, calcium is yellow, and magnesium is purple.

Ba−O peak for the central region of the nanoparticle is 2.69 Å; range 2.6−2.8 Å (RDF not shown), indicating that regions under high strain are located mainly at the (near) BaO/MgO interface region. Clearly, owing to the high proportion of ions at interfacial or near interfacial regions, these regions, compared with their bulk counterparts, weight heavily the average Ba−O bond distances.

At the surface, the BaO nanoparticle exposes (001) facets, which is not surprising since, for rocksalt-structured oxides, they are the most stable. Conversely, at the interfacial (encapsulated) regions, the BaO morphology is spherical, which implies the exposure of higher index (and energetically less stable) facets. We suggest therefore that the host MgO lattice helps stabilize these surfaces via energetically favorable cation−anion interactions. It is apparent that by encapsulating a nanoparticle, one can fabricate profoundly different crystal morphologies. Here, the BaO nanoparticles exhibit a hemispherical morphology.

CaO in MgO(perfect)/MgO(001): +13% Lattice Misfit. The simulated results for CaO encapsulation are summarized in Figure 3. Figure 3a shows a small segment of the simulation cell with part cut away enabling visualization of the nanoparticle. In Figure 3b, the surface of the MgO host is shown (white) together with the nanoparticle (blue) protruding out of the surface; the inset shows the morphological structure of the CaO nanoparticle. The figure shows that the surface of the MgO is not monatomically flat; rather, surface steps are present together with various MgO clusters and vacancies. Analysis of the CaO morphology, using graphical techniques, reveals that the nanoparticle exposes {100}, {110}, and {111} facets at the interfacial regions.

Parts c−e of Figure 3 show thin slices cut through the system along [100], [010], and [001], respectively. The CaO nanoparticle is oriented in accord with the encapsulating MgO lattice; interfaces conforming to CaO{100}/MgO{100} are evident. However, the nanoparticle is observed to have rotated by approximately 6° about [100], resulting in vicinal interfaces; no rotation about [010] or [001] is evident.

Inspection of epitaxial configurations along the interfacial planes reveals that the CaO and MgO planes are in alignment across much of the interfacial regions and facilitated by energetically favorable cation−anion interactions. However, because of the high (+13%) lattice misfit between the CaO and MgO, alignment across the whole interfacial region cannot be sustained.[27,28] Accordingly, dislocations evolve (as indicated by the arrows), which reside in regions of misalignment.

We now consider the structure of two nanoparticles, SrO followed by MgO, encapsulated within a BaO host lattice, which comprises a complex microstructure. As alluded to in the methods section, the simulation strategy was designed to ensure the "synthesis" of a host, which comprises a complex microstructure (Figure 1). This was achieved by annealing the host BaO lattice on top of an MgO substrate. The considerable lattice misfit between the BaO and MgO results in the evolution of a network of screw-edge dislocations within the BaO host lattice.

SrO in BaO(microstructure)/MgO(001): −7% Misfit. Parts a and b of Figure 4 show the surface structure of the BaO host lattice with the SrO nanoparticle at the center (the SrO nanoparticle morphology is inset). Thin slices, cut through the system, along [100], [010], and [001], respectively, are depicted in Figure 4c−e and show that the SrO nanoparticle exhibits complete registry with respect to the BaO host. In contrast to the systems above, the nanoparticle does not rotate with respect to the encapsulating lattice and complete registry between the two oxides is maintained. Screw-edge dislocations have evolved within the BaO host during the recrystallization process (as desired) and can be attributed to the high lattice misfit between the BaO thin film and the underlying MgO substrate. However, the dislocation cores do not encroach into the SrO nanoparticle; rather, if one inspects Figure 4e, one can observe, as indicated by the arrow in the figure, an edge dislocation that terminates at the interface between the SrO nanoparticle and the BaO host. In comparison with the previous systems, the defect structure is less complex and comprises small concentrations of Sr and Ba substitutionals, which reside in near interfacial (1−2 planes) regions.

Nearest neighbor Sr−O distances within the nanoparticle are calculated to be 2.6 Å, range 2.2−2.9 Å (RDF, Figure 4f; a_{SrO} = 2.58 Å) indicating that regions of the nanoparticle are under both compression and tension. However, the RDF provides little information pertaining to the strain profile. For example, dislocations, defects, and in particular the interfacial regions are likely to generate quite complex strain profiles. Accordingly, we use graphical techniques to extract more information from the simulation: In Figure 5a, a slice cut through the system

(27) Dong, L.; Schnitker, J.; Smith R. W.; Srolovitz, D. J. *J. Appl. Phys.* **1998**, *83*, 217.
(28) Ernst, F.; Recnik, A.; Langjahr, P. A.; Nellist, P. D.; Ruhle, M. *Acta Mater.* **1999**, *47*, 183.

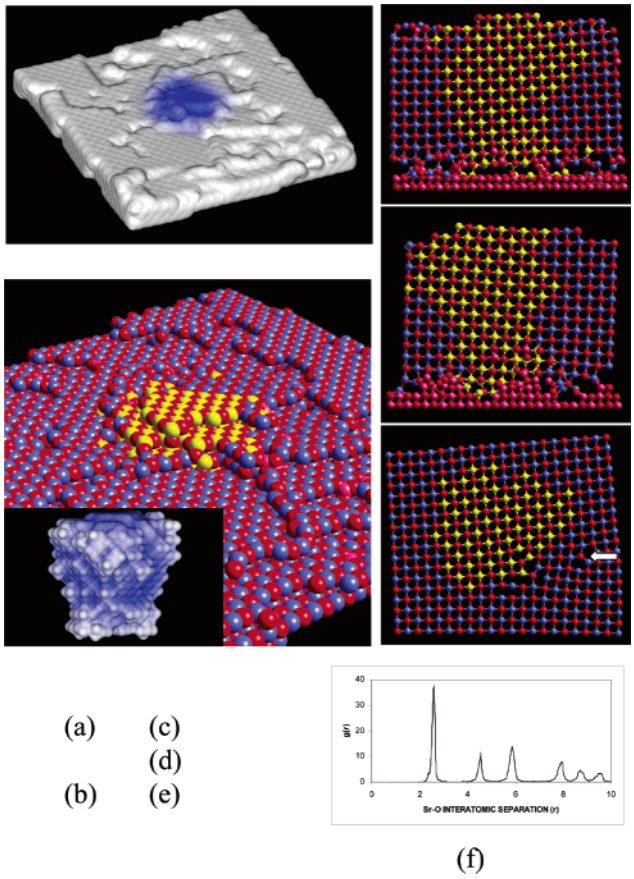

Figure 4. (a) Surface rendering model of the uppermost layers of the simulation cell for the SrO nanoparticle encapsulated within a microstructural BaO host lattice supported on an MgO substrate; (b) sphere model representation of the surface region of the simulation cell (the morphology of the nanoparticle is inset); (c−e) thin slices cut through the system and viewed along [100], [010], and [001], respectively; (f) calculated Sr−O RDF. Oxygen is colored red, strontium is yellow, barium is blue, and magnesium is purple.

viewing along [001] is depicted. Here, the bonding tolerance was set at 97%. Consequently, domains that are bonded indicate that these regions are compressed by at least 3%. It is interesting to note that very few of the Sr−O bonds within the nanoparticle are compressed. In Figure 5b, a small segment of the encapsulated SrO nanoparticle is shown, viewed along [001]. Here, the bonding tolerance was set at >103%, and therefore regions comprising unbonded cations and anions (as indicated by the arrows in the figure) indicate areas that are constrained under tension. It is clear that while the nanoparticle is mainly tensioned, the encapsulating BaO host oxide is compressed (along [100] and [010]). Such behavior aids the alignment of the SrO and BaO at the interfacial regions. We suggest that the energy associated with tensioning the SrO nanoparticle is outweighed by the favorable cation−anion interactions maintained across the SrO/BaO interfacial regions. In Figure 5c, a surface-rendering model of a slice cut through the system and viewed along [001] is shown. Regions colored blue indicate areas where the cation−anion distances are <96% compared with the parent and are therefore compressed. The arrows in the figure illustrate the position of dislocation cores within the encapsulating BaO thin film. It is interesting to note, albeit not unexpected, that compressed regions are localized around the dislocation cores.

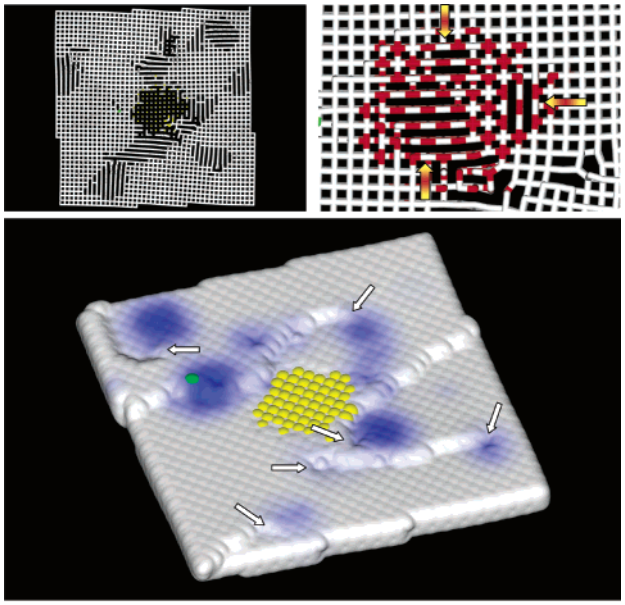

Figure 5. (a) Stick model representation of a slice cut through the simulation cell and viewed along [001] for the SrO nanoparticle encapsulated within a microstructural BaO host lattice; bonded domains indicate regions under compression (strontium ions are colored yellow); (b) an enlarged segment of (a) showing more clearly the encapsulated SrO nanoparticle (strontium is red); unbonded cations and anions (as indicated by the arrows) indicate areas that are constrained under tension; (c) surface rendering model of a slice cut through the system, viewed along [001]. The blue shading indicates compressed domains. The arrows locate dislocation cores within the host BaO lattice (strontium ions are yellow).

MgO in BaO(microstructure)/MgO(001): −28% Misfit. Figure 6a shows the MgO nanoparticle encapsulated within BaO. The oxides have clearly recrystallized back into the rocksalt structure. However, the orientation of the nanoparticle with respect to the host lattice is markedly different from the previous three systems. In particular, the nanoparticle appears to have separated at the center. The bottom segment has recrystallized to extend the structure of the supporting MgO, which one might have reasonably predicted. Conversely, the top has rotated. In particular, the MgO appears to have rotated by about 45° about [100] (Figure 6c). Additionally, the MgO has rotated by about 8° about [001] (Figure 6e). There is no appreciable rotation about [010] (Figure 6d).

No dislocations are observed to form within the MgO nanoparticle. However, a dislocation network (microstructure) is present within the encapsulating BaO lattice. These dislocations have mixed screw-edge character and are similar in structure to those identified in previous studies.[23]

Within the "bulk" of the MgO nanoparticle and encapsulating BaO lattice, the structures are relatively nondefective. Conversely, many defects can be observed at the interfacial and near interfacial regions and comprise mainly substitutional defects: Ba substituting for Mg at Mg sites with Mg ions displaced occupying vacant Ba sites.

Nearest neighbor Mg−O distances within the nanoparticle are calculated to be 2.05 Å, range 1.8−2.5 Å (RDF, Figure 6f; $a_{MgO} = 2.10$ Å) indicating that regions of the nanoparticle are under both compression and tension.

Table 2. Summary of the Main Structural Features Associated with Each of the Four Systems Considered in This Study: a_{NANO}, the Lattice Parameter of the Nanoparticle of the "Bulk" Parent Material; a_{HOST}, the Lattice Parameter of the "Bulk" Host; F_{NANO}, the Lattice Misfit Associated with the Nanoparticle and Encapsulating Lattice (eq 1); F_{INT}, the Misfit Associated with the Thin Film and Underlying MgO Substrate (eq 1); Orientation, the Rotation of the Nanoparticle with Respect to the Encapsulating Lattice about [100], [010], and [001]; M−O Distance, the Calculated (from RDF) Nearest Neighbor M−O Distances within the Nanoparticle and Host Lattice Together with the Range of Values Observed; Configuration, Epitaxial Relationships Identified to Exist between the Nanoparticle and Encapsulating Lattice

					orientation			M–O distance (RDF) (Å)		
system	$a_{NANO}/2$ (Å)	$a_{HOST}/2$ (Å)	F_{NANO}	F_{INT}	[100]	[010]	[001]	NANO	HOST	configuration
BaO in MgO	2.77	2.10	+28		8	6	3	2.65 2.3−3.2	2.1 1.9−2.3	no aligned regions: commensurate 4MgO/3BaO
CaO in MgO	2.40	2.10	+13		6	0	0	2.3 2.0−2.8	2.1 1.9−2.3	aligned regions separated by misfit dislocations
SrO in BaO	2.58	2.77	−7	+28	0	0	0	2.6 2.2−2.9	2.65 2.4−2.9	full alignment
MgO in BaO	2.10	2.77	−28	+28	43	2	8	2.05 1.8−2.5	2.65 2.4−2.9	no aligned regions: high angle grain boundaries

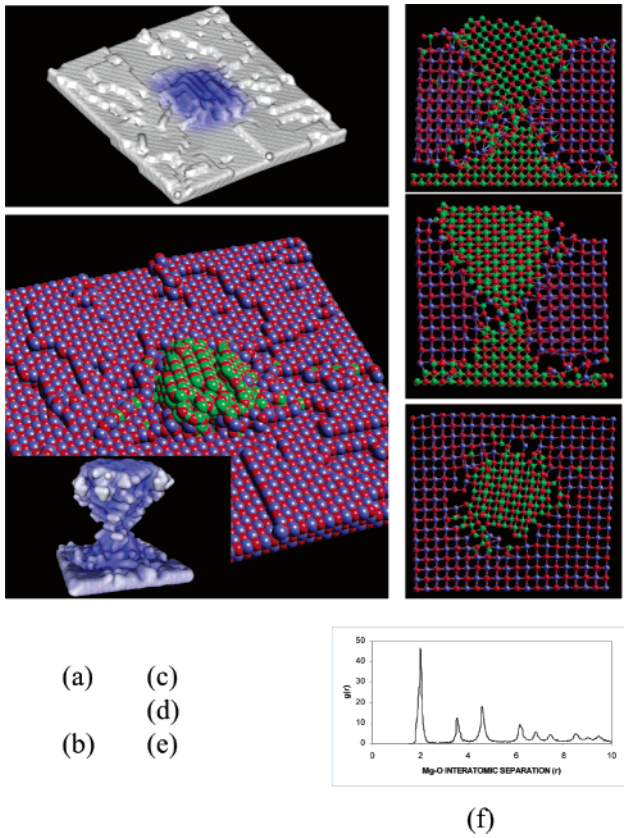

Figure 6. (a) Surface rendering model of the uppermost layers of the simulation cell for the MgO nanoparticle encapsulated within a microstructural BaO host lattice supported on an MgO substrate; (b) sphere model representation of the surface region of the simulation cell showing the protrusion of the MgO nanoparticle out of the surface of the encapsulating BaO lattice (nanoparticle morphology is inset); (c−e) thin slices cut through the system and viewed along [100], [010], and [001], respectively; (f) calculated Mg−O RDF. Oxygen is colored red, barium is blue, and magnesium is green.

The morphological appearance of the MgO nanoparticle is depicted in Figure 6f (inset). Inspection of the nanoparticle suggests that it exposes the (210) at the surface. However, owing to the small size of the nanoparticle including perhaps some additional faceting at the surface, assignation of interfacial boundaries between the nanoparticle and encapsulating BaO lattice would prove disingenuous.

Discussion

A summary of the main structural features associated with each of the four systems considered in this study is presented in Table 2.

Recently, there have been several studies in which the interface between two oxide materials has been investigated using high-resolution imaging techniques (for example see refs 28−31). A theme common to all these studies is that the authors have presented images showing clear atomistic detail of the interfacial region and core structures of misfit dislocations and stacking faults. Such images can be compared directly with the simulated (atomistic) models such as those presented here. In particular, experiment suggests that the lattice misfit and associated lattice stress within each system is quenched via the evolution of dislocation networks, the core structures[28,31] and periodicities[32] of which are similar to those we have predicted theoretically.[33]

More direct comparisons between this work and experiment can be made with the studies of Jeng and Shen,[34] who explored the structure and thermally activated rotation of $Ni_{1-x}O$ (denoted N) particles encapsulated within a CaO (denoted C) matrix. Specifically, CaO/$Ni_{1-x}O$ powders (4:1 molar ratio) were sintered and then annealed at various temperatures for long durations. Transmission electron microscopy was then employed to elucidate orientational configurations of the $Ni_{1-x}O$ with respect to the encapsulating CaO. The authors observed that the $Ni_{1-x}O$ particles reached "parallel epitaxial relationship, i.e., $[100]_N/[100]_C$, $[010]_N/[010]_C$", similar to our theoretical models. The authors propose also "$[010]_N/[011]_C$" or "45°-off epitaxy"; in this present study, the encapsulated MgO nanoparticle was observed to have rotated by about 45° with respect to the BaO host lattice.

(29) Wu, J. S.; Jia, C. L.; Urban, K.; Hao, J. H.; Xi, X. X. *J. Mater. Res.* **2001**, *16*, 3443.
(30) Lei, C. H.; Van Tendeloo, G.; Siegert, M.; Schubert, J. *J. Mater. Res.* **2002**, *17*, 1923.
(31) Jia, C. L.; Siegert, M.; Urban, K. *Acta Mater.* **2001**, *49*, 2783.
(32) Wang, A.; Belot, J. A.; Marks, T. J.; Markworth, P. R.; Chang, R. P. H.; Chudzik, M. P.; Kannerwurf, C. R. *Physica C* **1999**, *320*, 154.
(33) Sayle, D. C.; Catlow, C. R. A.; Dulamita, N.; Healy, M. J. F.; Maicaneanu, S. A.; Slater, B.; Watson, G. W. *Mol. Simul.* **2002**, *28*, 683.
(34) Jeng, M.-L.; Shen, P. *Mater. Sci. Eng.* **2000**, *A287*, 1. Jeng, M.-L.; Shen, P. *J. Solid State Chem.* **2000**, *152*, 421.

Van Huis et al., who explored the structural properties of Au and Ag nanoparticles (2−14 nm in size) embedded in the near surface region of MgO using ion implantation techniques, observed Au clusters with spherical morphologies and Ag clusters with octahedral morphologies. The authors present HRTEM images of the system with very clear atomistic detail. The orientations of the metal clusters are commensurate with that of the encapsulating MgO lattice, with "cube-on-cube" orientational relationships. Inspection of these images reveals alignment of the lattice planes of the MgO and metal ions, which is associated with an expansion of the metal lattices: the Au nanoparticles expanded by 0.4% and Ag by 0.9%, indicating that the nanoparticles are constrained under tension. Moreover, by close inspection of the HRTEM images, one can observe dislocations within the encapsulating MgO lattice. Although the systems considered in this present study are oxide/oxide rather than metal/oxide, the experimental results of Van Huis et al. do provide some support for the possibility of an oxide host lattice exacting a profound influence over the structure of an oxide nanoparticle when it is encapsulated.

An important observation associated with all the systems considered in this present study is that the bulk regions of the nanoparticles are crystalline and relatively defect-free in contrast to interfacial regions, which are highly defective, comprising substitutionals, vacancies, and interstitials. An experimental study by Lind et al. on the Fe_2O_3/NiO system[35] showed interdiffusion between the Fe_2O_3 and NiO to be of the order of only 1−2 atomic layers.

Conclusions

We have developed a viable simulation procedure for generating nanoparticles encapsulated within a host lattice that comprises a complex microstructure. The main strength associated with this method is that it enables the nanoparticles to adopt low-energy configurations relative to the host lattice and independent of the starting configuration. This is achieved by placing the nanoparticle within an amorphous host followed by annealing. Since the ionic mobility within the amorphous material is commensurate with a melt, the ions are able to move freely, enabling them to establish a much lower energy configuration. Essentially, exploration of the potential energy surface is more thorough facilitating a considerable acceleration of the dynamical simulation. Furthermore, by employing these large simulation cells the defect−defect interactions are modeled explicitly without recourse to further simulations.

This study shows that the nanoparticles are highly strained, which, as stated by Dye et al.,[21] "may influence strongly the mechanical and fatigue properties of the material". For example, within the SrO/BaO system, the SrO maintains full alignment with respect to the BaO host lattice. To accommodate such a configuration, the SrO is tensioned. We suggest that because of the small size of the nanoparticle, the energy terms associated with maintaining favorable interfacial interactions outweigh the energy terms associated with straining the SrO lattice. It therefore follows that if the size of the nanoparticle were to increase, at some particular point (critical nanoparticle size), the configuration could no longer be sustained as the number of bulk atoms increases faster than the number of interfacial ions with increasing nanoparticle sizes.

Such "critical sizes" are controlled ultimately by the lattice misfit associated with the system. Indeed, for the other three systems considered in this present study, which are associated with much higher lattice misfits compared with the SrO/BaO system, complete alignment of the nanoparticle with respect to the host lattice was not observed, suggesting that the sizes of these nanoparticles is greater than the critical size. And while partial alignment was observed in the CaO/MgO system (+13% separated by misfit dislocations), for the BaO/MgO system (+28% misfit), no regions of alignment were observed. For this latter system, a commensurate configuration evolved with four interatomic spacings of the MgO lattice matched with three interatomic spacings of the BaO. Rotations of the nanoparticle with respect to the host lattice were also observed, together with a wealth of defects at the interfacial regions, which help further reduce the influence of the lattice misfit, while maintaining energetically favorable interfacial configurations.

Critical thicknesses are well documented for supported thin films. Specifically, as the thin film thickness increases, so dislocations evolve to help quench the lattice stress. An elegant and convincing example of such behavior can be seen in the simulation work of Dong et al.[27] Additionally, in previous work we have suggested a similar effect, that of critical areas as applied to supported nanoparticles.[17] Since the presence of dislocations can influence profoundly the properties of the material, it is an important issue to address.

Another interesting feature is that the dislocation cores within the host lattice did not traverse into the nanoparticle; rather dislocations in the vicinity of the nanoparticle simply terminated at the nanoparticle/host interface. We suggest that a dislocation core traversing both the nanoparticle and host lattice is likely to destabilize the nanoparticle and was not therefore observed. However, it will be interesting to test this hypothesis by exploring more systems.

General trends indicate the bulk of the nanoparticle and encapsulating matrix are relatively defect-free compared with the highly defective interfacial regions. Specifically, we have observed substitutionals, vacancies, and interstitials including complex clustering of these point defects. Tasker and Stoneham have suggested that since low interfacial densities (associated with vacancies, interstitials, and substitutionals) give rise to low-energy configurations, "such species are not defects as such; rather they form an integral part of the low energy configuration".[36]

Acknowledgment. We acknowledge funding for a 20 processor Compaq SC cluster, located at the Rutherford Appleton Laboratory, which was purchased and supported with funding from the JREI (JR99BAPAEQ) and Compaq; CCP5 for a travel grant.

JA030119I

(35) Lind, D. M.; Berry, S. D.; Chern, G.; Mathias H.; Testardi, L. R. *Phys. Rev. B* **1992**, *45*, 1838.

(36) Tasker, P. W.; Stoneham, A. M. *J. Chemi. Phys.* **1987**, *84*, 149.